Improved device performance in *in-situ* SiN_x/AlN/GaN MIS-HEMTs with *ex-situ* Al_2O_3 passivation at elevated temperatures

Pradip Dalapati,[1,a)] Subramaniam Arulkumaran,[2] Hanlin Xie,[3,4] Geok Ing Ng[1,2,3,4,a)]

[1]School of Electrical and Electronic Engineering, Nanyang Technological University, 50 Nanyang Avenue, Singapore 639798, Republic of Singapore
[2]Temasek Laboratories@NTU, Nanyang Technological University, Research Techno Plaza, 50 Nanyang Drive, Singapore 637553, Republic of Singapore
[3]Institute of Microelectronics (IME), Agency for Science, Technology and Research (A*STAR), 2 Fusionopolis Way, Innovis #08-02, Singapore 138634, Republic of Singapore
[4]National GaN Technology Centre (NGTC), Agency for Science, Technology and Research (A*STAR), 2 Fusionopolis Way, Innovis #08-02, Singapore 138634, Republic of Singapore
[*a)]Authors to whom correspondence should be addressed: pradip.dalapati@ntu.edu.sg and eging@ntu.edu.sg

ABSTRACT

In the present work, the role of *ex-situ* Al_2O_3 passivation in *in-situ* SiN_x/AlN/GaN metal–insulator–semiconductor high-electron-mobility transistors (MIS-HEMTs) to boost device performance and thermal stability during the high-temperature operations has been thoroughly investigated. At room temperature (RT), the MIS-HEMT fabricated with an atomic layer deposited (ALD)-Al_2O_3 (MIS-HEMT B) exhibits higher maximum drain current ($I_{d,max}$), peak transconductance ($g_{m,max}$), and lower subthreshold slope (*SS*) and gate leakage current compared to MIS-HEMT A fabricated without *ex-situ* Al_2O_3, signifying the effectiveness of ALD-Al_2O_3 layer to passivate severe surface states. Noted, when the temperature rises from 298 to 423 K, the values of $I_{d,max}$, and $g_{m,max}$ decrease noticeably, while *SS* and gate leakage current increase considerably in both MIS-HEMTs A and B. However, MIS-HEMT B demonstrates a lower degradation rate in various device properties at 423 K compared to MIS-HEMT A, implying that ALD-Al_2O_3 passivation improves thermal stability. Additionally, ALD-Al_2O_3 passivation reduces the interface state density from 7.48×10^{12} to 5.3×10^{12} $cm^{-2}.eV^{-1}$, highlighting its critical role in improving overall device performance.

With the advantageous features of an ultrawide bandgap, high critical electric field, and excellent chemical and thermal stability, AlN/GaN HEMTs are inherently desirable for applications in high-power, high-frequency and high-temperature electronics.[1–5] The traditional AlGaN/GaN HEMTs with the optimized AlGaN barrier thickness (~ 20−40 nm) suffer from lower gate control capability and strong short channel effects occur during the gate length scaling.[6] On the other hand, the AlN/GaN HEMTs with an ultrathin (3–5 nm) barrier layer can greatly improve gate response and effectively mitigate short-channel effects.[3,6] In addition, the high band offset and enormous polarization discontinuity between AlN and GaN layers induce a high density of two-dimensional electron gas (2DEG) in the AlN/GaN heterostructure, facilitating the HEMTs for its outstanding high-frequency operations.[1,4,6]

For further technological advancement, the *in-situ* deposition of SiN_x layer by metal-organic chemical vapor deposition (MOCVD) just after the AlN/GaN structure is essential.[7] In the AlN/GaN heterostructure, the *in-situ* SiN_x takes a paramount role in protecting the 2DEG properties, ensuring excellent device performance.[4,7] The deposition of *in-situ* SiN_x gate insulator layer via MOCVD can provide a high-quality dielectric film and significantly lower interface trap states when compared with other *ex-situ* dielectric films, which in turn help to suppress the gate leakage in MIS-HEMT.[8] The inclusion of *in-situ* SiN_x gate dielectric has been shown to expressively attenuate the surface states, thereby mitigating the deleterious impacts of surface states-related scattering mechanisms on electron mobility.[4,9] It is noteworthy that additional *ex-situ* surface passivation can accomplish an immense contribution to unlock the full potential of *in-situ* SiN_x/AlN/GaN MIS-HEMTs.[4,7] Interestingly, studies on the impacts of *ex-situ* surface passivation, especially in *in-situ* SiN_x/AlN/GaN MIS-HEMTs, are rather few.[4,7]

Due to the efficient heat spreading capability of AlN, the SiN_x/AlN/GaN MIS-HEMT is believed to

be favorable in diverse applications, particularly at high-temperature (HT) environments, such as automotive or aerospace electronic systems.[1,10] Henceforth, to realize a highly reliable and stable *in-situ* SiN_x/AlN/GaN MIS-HEMT during high-temperature operations, it is important to rigorously perform device characterizations and thoroughly understand the device properties at elevated temperatures.[10] Furthermore, over the last few decades, studies on the high-temperature characteristics of AlGaN/GaN-based HEMTs or MIS-HEMTs with different gate dielectric layers have been extensively undertaken,[11–14] whereas the similar studies on AlN/GaN HEMTs or SiN_x/AlN/GaN MIS-HEMTs are very limited.[3,15–17] Hence, the effects of HT on different device properties of *in-situ* SiN_x/AlN/GaN MIS-HEMTs, both with and without *ex-situ* surface passivation, need further investigation.

Therefore, with this goal in mind, we have fabricated *in-situ* SiN_x/AlN/GaN MIS-HEMTs without and with *ex-situ* Al_2O_3 passivation by ALD and perform device characterizations rigorously at elevated temperatures. Nevertheless, to understand the correlation between temperature-dependent interface trap states and different device parameters of the fabricated MIS-HEMTs without and with *ex-situ* Al_2O_3, the interface state density (D_{it}) of *in-situ* SiN_x/AlN/GaN MIS-diodes (with and without *ex-situ* Al_2O_3) has been investigated through frequency-dependent conductance measurements at different temperatures.

In the present work, the *in-situ* SiN_x gate dielectric and the main III-nitride materials (AlN/GaN) were grown by MOCVD on a 6-inch Si (111) substrate. The cross-sectional schematic structures of the fabricated MIS-HEMTs without (MIS-HEMT A) and with *ex-situ* ALD-Al_2O_3 (~ 10 nm) are illustrated in Figs. 1(a) and 1(b), respectively.

MIS-HEMTs were fabricated with different device fabrication steps, such as a photolithographic process under UV light, a mesa isolation process with reactive ion etching (gas plasma: Cl_2/BCl_3), an electron beam evaporation step for the formation of different contact pads, and a high-temperature annealing process. Noted, the ALD-Al_2O_3 surface passivation layer was deposited at 250 °C. More details about the fabrication processes of MIS-HEMTs are described in our previous works.[4,7,18] The temperature-dependence device characterizations, including DC output and transfer characteristics of MIS-HEMTs, as well as frequency-dependent conductance measurements of MIS-diodes, were carried out by using a power device analyzer (Agilent B1505A). This analyzer was connected to the high-voltage probe station under an electrically shielded condition and high-temperature controller.

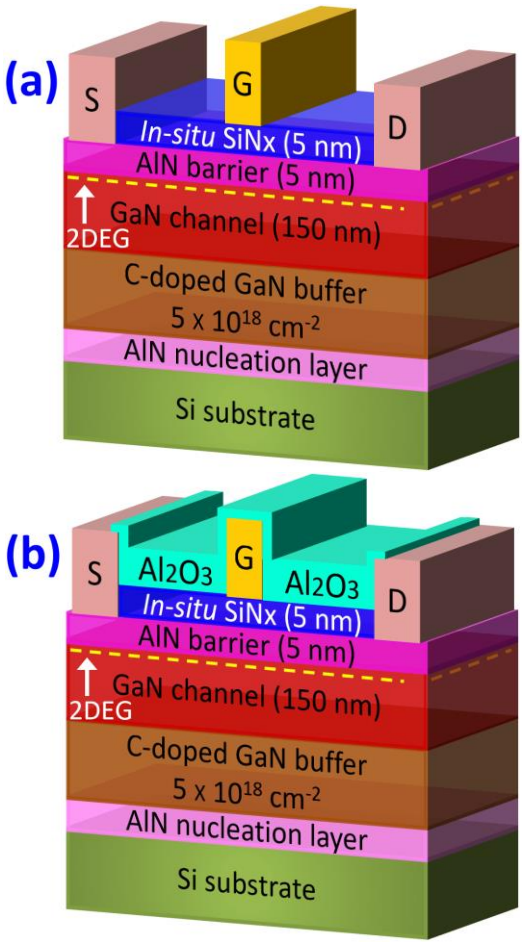

FIG. 1. Cross-sectional schematic structure of *in-situ* SiN_x/AlN/GaN MIS-HEMTs (a) without (MIS-HEMT A), and (b) with ALD-Al_2O_3 passivation layer (MIS-HEMT B). Device dimensions: MIS-HEMTs = $L_g/L_{sg}/L_{gd}/W_g$ = 2/2/2/(2 × 50) µm; diameter of the circular MIS-diodes = 100 µm.

In order to investigate the effectiveness of the *ex-situ* Al_2O_3 passivation layer to improve the DC output performance of *in-situ* SiN_x/AlN/GaN MIS-HEMTs, by achieving higher $I_{d,max}$, and lower static on-resistance (R_{on-s}), and better thermal stability, we measured the DC output (I_d-V_d) and transfer characteristics of MIS-HEMTs A and B at 298-423 K (see Fig. S2, supplementary material). The variations of different device parameters are displayed in Fig. 2.

Intriguingly, the values of $I_{d,max}$ at V_g = 2 V (938.04 mA/mm) and $g_{m,max}$ (229.1 mS/mm) in MIS-HEMT B are higher than MIS-HEMT A (853.44 mA/mm and 198.74 mS/mm) at RT. The significantly higher $I_{d,max}$, and $g_{m,max}$ in MIS-HEMT B could be ascribed to the improved 2DEG density by the ALD-Al_2O_3 surface passivation as observed in Refs. 4 and 7.

Nevertheless, Figs. 2(a) and 2(b) show that at 423 K, the values of $I_{d,max}$ ($g_{m,max}$) in MIS-HEMTs A and B decrease to 699.22 (149.94) and 794.74 mA/mm (182.34 mS/mm), respectively. The significant reduction in $I_{d,max}$, and $g_{m,max}$ could be attributed to the lowering of 2DEG mobility and effective electron velocity at HT as claimed in Refs. 11 and 19. Furthermore, it is reported that at HT, the concentration of phonon increases rapidly which in turn increases the scattering effect and degrades the 2DEG mobility of the employed epitaxial structure.[11–13] Previous reports suggest that the variation of 2DEG sheet carrier density is almost insensitive to temperature, particularly in AlN/GaN heterostructures, whereas the 2DEG mobility decreases strongly at exacerbated temperature.[16,20] Based on these results, the authors claimed that the variation of conduction process with temperature is strongly associated with the change of 2DEG mobility as a function of temperature at AlN/GaN heterostructures.[16,20]

When temperature increases from 298 K to 423 K, $I_{d,max}$ ($g_{m,max}$) degrades by about 18.7% (24.55%) in MIS-HEMT A, whereas MIS-HEMT B exhibits a lower degradation rate in $I_{d,max}$ ($g_{m,max}$) of about 15.28% (20.41%). This lower degradation rate in MIS-HEMT B suggests that the thermal stability is improved due to effective surface passivation by the ALD-Al_2O_3 layer. The effective surface passivation can improve the interface quality by lowering interface trap states in such devices and decline the scattering phenomenon, as a result, higher 2DEG mobility.[18,21,22] Deng *et al.* reported that in AlGaN/GaN HEMTs, the inclusion of SiN_x deposited by the low-pressure chemical vapor deposition helps to reduce surface trapping states, as a result, the thermal stability of the device improves noticeably.[23] Tan *et al.* have also noticed that after the deposition of AlN/SiN_x bi-layer as the passivation dielectrics, the thermal stability improves greatly in AlGaN/GaN HEMTs.[22] Therefore, we believe that the improved interface quality in MIS-HEMT B with an ALD-Al_2O_3 surface passivation helps to reduce the degradation rate of 2DEG mobility at HT in a better way compared to MIS-HEMT A, and hence, improve the thermal stability. Recently, the auspicious role of ALD-Al_2O_3 passivation layer to reduce the interface trap density at the Si/SiO_2/Al_2O_3 interfaces and enhance the thermal stability has also been studied in Ref. 24. However, the role of ALD-Al_2O_3 surface passivation to improve the interface quality in *in-situ* SiN_x/AlN/GaN MIS-HEMTs is discussed below.

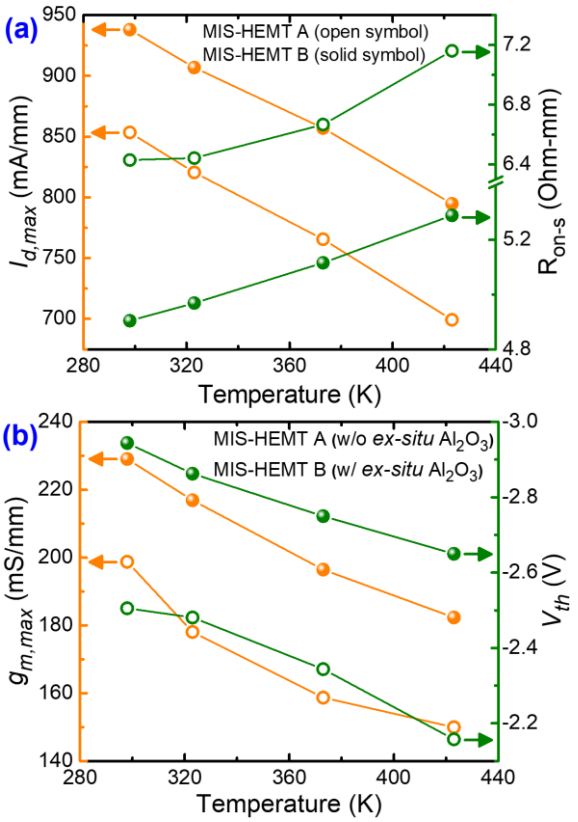

FIG. 2. (a) Values of $I_{d,max}$ and R_{on-s} in MIS-HEMT A (open symbol) and MIS-HEMT B (solid symbol) at different temperatures. (b) Values of $g_{m,max}$ and V_{th} in MIS-HEMT A and MIS-HEMT B at different temperatures.

The presence of a large number of interface traps plays a critical role not only to deplete the 2DEG through severe Coulomb scattering but also to improve the on-resistance.[9,25] Hence, to reduce the interface traps, the surface passivation layer can take an important role, mainly in AlN/GaN HEMTs.[4,9,25] In this work, due to excellent surface passivation in MIS-HEMT B with an *ex-situ* Al_2O_3 dielectric film, the estimated value of R_{on-s} from I_d-V_d characteristics at RT reduces pointedly from 6.43 (MIS-HEMT A) to 4.9 Ohm-mm (see Fig. 2(a)). Before surface passivation,

several unfilled bonds of N in SiN_x can exist.[4] These unfilled bonds of N might act as trap centers and worsen the device performance through severe charge trapping. After the inclusion of an *ex-situ* Al_2O_3 passivation layer, the pre-existed unfilled bonds of N in SiN_x can be filled by Al atoms (formation of Al-N bonds) and improve the surface quality (see the X-ray photoelectron spectroscopy results in section S1, supplementary material).

Noted, the value of R_{on-s} at 423 K is increased by almost 11.35% and 7.96% in MIS-HEMTs A and B, respectively. In Al_2O_3/AlGaN/GaN-based metal-oxide-semiconductor field-effect transistor (MOS-FET), R_{on-s} increases markedly from 16.3 to 36.4 Ohm-mm when the temperature increases from 300 to 573 K.[19] In another work, the authors observed that in AlGaN/GaN HEMTs, the value of R_{on-s} is significantly higher (15.4 Ohm-mm) at 398 K than the room temperature value (11 Ohm-mm), supporting our observations in Fig. 2(a).[11] In addition, based on the obtained results, we believe that in MIS-HEMT B, *ex-situ* Al_2O_3 passivates the surface traps extensively, mainly in the gate to drain access region, leading to a smaller degradation rate in R_{on-s}.

Furthermore, based on the temperature-dependent I_d-V_g results at V_d = 4 V (see Figs. S2(c)-S2(d), supplementary material), we have estimated the threshold voltage (V_{th}) in MIS-HEMTs A and B. The obtained values of V_{th} in MIS-HEMTs A and B at different temperatures are displayed in Fig. 2(b). After the inclusion of an ALD-Al_2O_3 passivation film in MIS-HEMT B, V_{th} shifts towards a more negative value compared to MIS-HEMT A. Prior reports also suggest that the inclusion of a passivation layer can shift V_{th} in such devices towards a more negative value i.e., a greater gate voltage is required to deplete the channel.[4,7,26,27] The higher negative V_{th} in passivated HEMTs could be associated with the improved 2DEG carrier density.[4,7,26,27] Moreover, when the temperature increases from 298 to 423 K, V_{th} shifts from -2.51 V (-2.94 V) to -2.16 V (-2.65 V) in MIS-HEMT A (MIS-HEMT B). The obtained results suggest that the shift of V_{th} (ΔV_{th}) is slightly higher in MIS-HEMT A (340 mV) compared to MIS-HEMT B (290 mV). It is reported that the positive shift of V_{th} with temperature could be related to the improved carrier trap density at HT.[28] In addition, the authors in Ref. 28 have confirmed the carrier trapping effects at HT through the temperature-dependent leakage current characteristics in AlGaN/GaN HEMTs. Therefore, we can infer that the higher ΔV_{th} in MIS-HEMT A might be attributed to the larger D_{it}, which we discuss below.

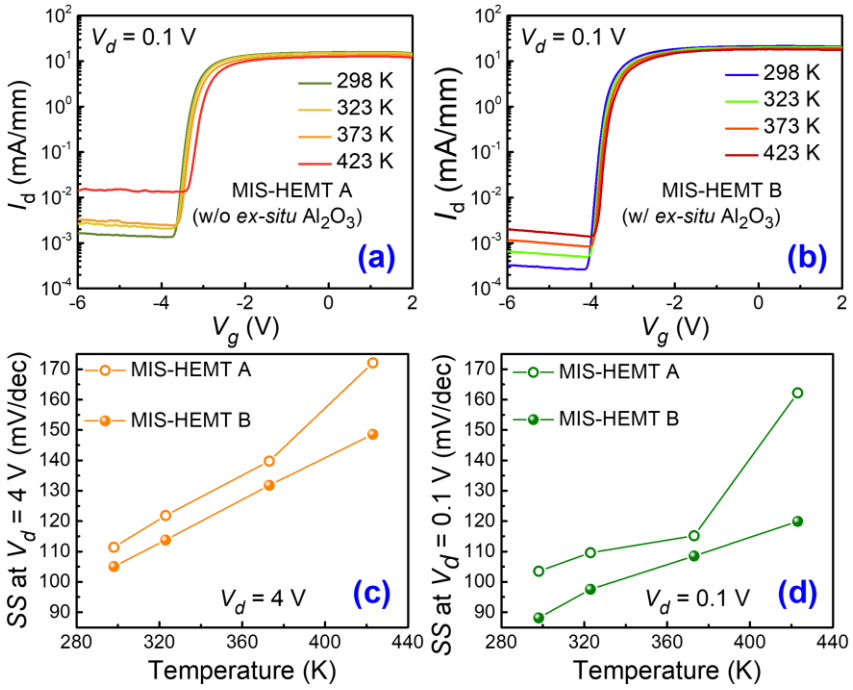

FIG. 3. DC transfer characteristics of (a) MIS-HEMT A, and (b) MIS-HEMT B at V_d = 0.1 V. Values of *SS* at different temperatures ((c) V_d = 4 V, and (d) V_d = 0.1 V).

To compare the subthreshold characteristics of MIS-HEMTs A and B at a lower drain bias, the I_d-V_g measurements at V_d = 0.1 V have also been performed at different temperatures (see Figs. 3(a) and (b)). The calculated values of subthreshold slope in MIS-HEMTs A and B at different temperatures are portrayed in Figs. 3(c) and 3(d), respectively (V_d = 4 and 0.1 V). It is suggested that the high interface trap states in AlGaN/GaN HEMTs can drastically increase *SS*.[29] It is noteworthy in Fig. 3 that *SS* in MIS-HEMT B is notably lower even at the high temperature compared to MIS-HEMT A, indicating better interface quality with the ALD-Al_2O_3 passivation layer. Koehler *et al.* have also observed that the surface passivation by different dielectric films helps to reduce D_{it} in AlGaN/GaN HEMTs, as a result, *SS* decreases noticeably, supporting our results in Fig. 3.[30]

Additionally, to examine how the gate leakage current in MIS-HEMTs A and B varies with temperature, we measured the gate current (I_g) as a function of the gate-source voltage (V_{gs}) at different temperatures (V_d = 0.1 V) as illustrated in Fig. 4. MIS-HEMT B exhibits significantly lower leakage current compared to MIS-HEMT A. For say, at 298 K (423 K), the gate leakage currents in MIS-HEMTs A and B are 4.78×10^{-7} mA/mm (2.32×10^{-6} mA/mm), and 1.12×10^{-7} mA/mm (5.43×10^{-7} mA/mm), respectively (V_{gs} = -6 V). The authors in Refs. 31 and 32 have also noticed that after the inclusion of a surface passivation layer in such devices, I_g reduces greatly, supporting our observation in Fig. 4.

It is reported that the presence of numerous surface and interface trap states plays a critical role in gate leakage.[32–35] During high-temperature operation of such devices, severe gate leakage current becomes increasingly significant. Under off-state conditions (high electric field), several parasitic electrons might be pumped from the gate metal to the surface of SiN_x, where they can easily become trapped at surface states, worsening the gate characteristics. However, the measured I_g-V_{gs} curves at different temperatures suggest that the *ex-situ* Al_2O_3 passivation can take an important role to prevent severe electron trapping at the surface states and improve the gate characteristics of MIS-HEMT B. Importantly, the presence of an *ex-situ* Al_2O_3 passivation layer in MIS-HEMT B can regulate the electric field line distribution, mainly between the gate and drain electrodes, which in turn helps to decrease the leakage current (see Fig. 4(b)).[31,32] Additionally, the ALD-Al_2O_3 passivation can keep several trap states on the device surface away from the gate electrode in MIS-HEMT B and decline gate leakage.[32] Furthermore, several conduction mechanisms, such as thermionic emission (TE), Poole–Frenkel emission (PFE), 2D-VRH, Fowler–Nordheim tunneling (FNT), trap-assisted tunneling (TAT), and defect-assisted tunneling (DAT) can be responsible for the gate leakage current.[35–37] Dutta *et al.* have comprehensively investigated the gate leakage mechanisms in AlInN/GaN and AlGaN/GaN MIS-HEMTs with SiN_x as gate dielectric and found that the PFE current is the dominant leakage process at higher reverse bias, whereas TAT and FNT play the main role at low to medium forward bias and higher forward bias, respectively.[37] In addition, at very low reverse and forward bias voltages, DAT mechanism is dominated.[37] Similar observations have also been reported by Liu *et al.* in AlGaN/GaN MIS-HEMTs with ALD-Al_2O_3 as gate dielectric.[38]

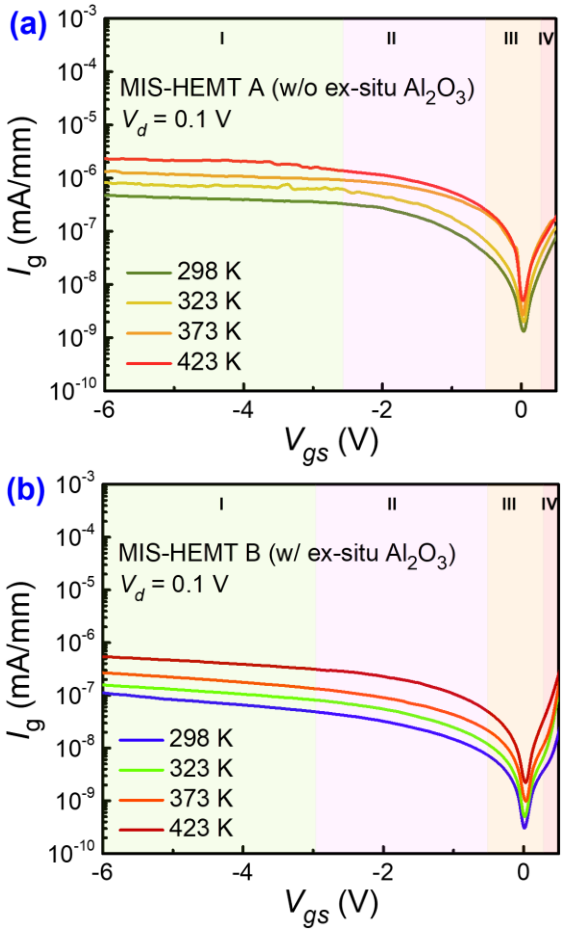

FIG. 4. I_g-V_{gs} curves at different temperatures for (a) MIS-HEMT A, (b) MIS-HEMT B.

However, we believe the combined effects of PF emission (Region I, $V_{gs} > V_{th}$), TAT (Regions II and IV, $V_{gs} < V_{th} >$ -0.5 V and $V_{gs} >$ 0.3 V) and DAT (Region III, V_{gs} within - 0.5 to 0.3 V) are the leading conduction mechanisms for the gate leakage current in our devices (details are described in the supplementary material).[33,35] Recently, Kumar *et al.* have observed that the existence of several oxygen vacancies in the oxide-based gate stack strongly contributes to PF emission current.[35] Therefore, in our devices, the presence of many nitrogen vacancies in the SiN_x gate dielectric could contribute largely to the leakage process. Under the high electric field, the lowering of activation energy (barrier) of traps leads to severe leakage current through PF emission.[39] The presence of several defect states in our devices can lead to increased leakage current through TAT and DAT conduction processes, where charge carriers move by hopping (trap to trap) or capture emission.[40]

Furthermore, it is noted that the lower gate leakage current could improve the breakdown voltage characteristics of the device.[32] To validate this point and shed more light on this issue, we measured the breakdown voltage characteristics of MIS-HEMTs A and B (see supplementary material). Interestingly, the breakdown voltage of MIS-HEMT B is higher (166 V) than that of MIS-HEMT A (141 V), supporting the above statement.

Moreover, it is important to mention that in MIS-HEMTs, gate leakage processes are greatly affected by the existence of high-density interface traps at the interface between the gate dielectric and III-Nitride.[37] Therefore, it could be of great interest to investigate the interface trap density for both devices at HT, which we consider next.

To evaluate the temperature dependence of D_{it} in *in-situ* SiN_x/AlN/GaN MIS-diode A (without *ex-situ* Al_2O_3 passivation) and MIS-diode B (with *ex-situ* Al_2O_3 passivation), we measured the frequency-dependent conductance characteristics at 298-423 K and the results are displayed in Fig. 5. We applied the gate voltage close to the vicinity of V_{th}. When we applied the gate voltage close to V_{th}, the traps, distributed randomly at the AlN/GaN interface, can quickly respond to AC signals and give rise to a G_p/ω peak (see Figs. 5(a) and 5(b)). Thus, we estimated D_{it} at the AlN/GaN interface from the peak regions in the G_p/ω versus ω plots (details of the calculations are mentioned in our earlier work).[18] The variation of D_{it} with temperature is shown in Fig. 5(c). The calculated values of D_{it} in MIS-diode A at RT and 423 K are about 7.48×10^{12} and 11.34×10^{12} $cm^{-2}.eV^{-1}$, respectively. The room temperature result is consistent with the reported value of D_{it} at AlN/GaN interface in *in-situ* SiN_x/AlN/GaN MIS-diodes (thickness of *in-situ* SiN_x: 7 nm).[41] However, it is worth noticing that after *ex-situ* Al_2O_3 passivation, MIS-diode B exhibits much lower D_{it} (5.3×10^{12} $cm^{-2}.eV^{-1}$ at 298 K, and 7.81×10^{12} $cm^{-2}.eV^{-1}$ at 423 K). The obtained results suggest that *ex-situ* passivation has a strong influence on the access region of MIS-HEMT B, which helps to suppress D_{it}. The reduction of interface trap states with excellent passivation has also been observed in the prior publications.[18,25] A detailed explanation of the effect of surface passivation in the access region of GaN-based MIS-HEMTs can be found in Ref. 25.

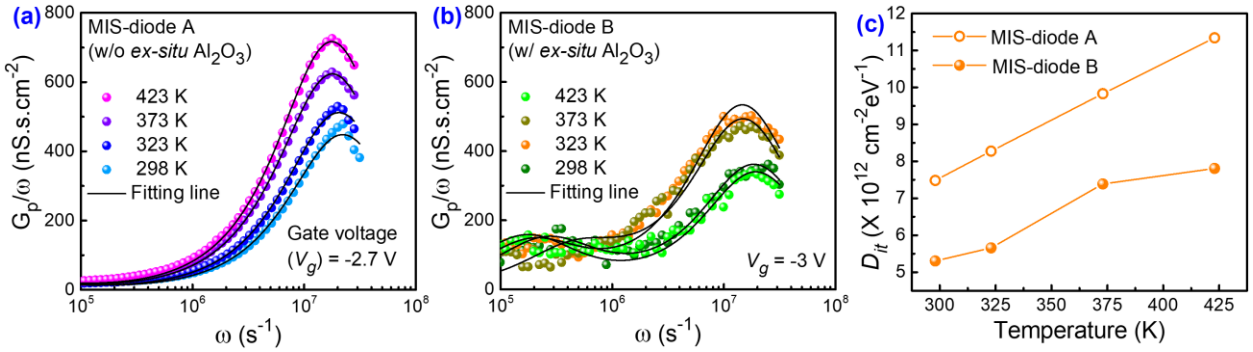

FIG. 5. G_p/ω versus ω plots for (a) MIS-diode A (without *ex-situ* Al_2O_3 passivation layer), (b) MIS-diode B (with *ex-situ* Al_2O_3 passivation layer). (c) Variation of D_{it} with temperature.

Additionally, the reduction in D_{it} with *ex-situ* Al_2O_3 passivation helps to decline the current collapse (CC) and dynamic on-resistance (dR_{on}) in MIS-HEMT B. The estimated values of CC and dR_{on} in MIS-HEMT B (MIS-HEMT A) are about 20% (29%) and 6.25 (9.82) Ohm-mm, respectively (see supplementary material). A similar reduction in CC and dR_{on} in AlGaN/GaN HEMTs with an AlN passivation layer has also been reported elsewhere.[42]

In our earlier work,[18] we have also noticed that the reduction of different electronic states near the interfaces can decline the leakage current significantly in such devices, supporting our present work as well. Moreover, based on the obtained results, we believe that the reduction of interface trap states with *ex-situ* Al_2O_3 passivation greatly helps to improve the device performance and thermal stability in *in-situ* SiN_x/AlN/GaN MIS-HEMTs.

In this work, the role of *ex-situ* Al_2O_3 passivation in *in-situ* SiN_x/AlN/GaN MIS-HEMTs to enhance device performance and thermal stability during high-temperature operations has been investigated. In MIS-HEMT B (with *ex-situ* Al_2O_3 passivation layer), the values of $I_{d,max}$, and $g_{m,max}$ at RT are significantly higher compared to MIS-HEMT A (without *ex-situ* Al_2O_3 passivation layer). The improvement in $I_{d,max}$, and $g_{m,max}$ could be attributed to the increased 2DEG density by the ALD-Al_2O_3 passivation layer. *Ex-situ* Al_2O_3 plays a vital role in reducing interface trap states, which subsequently lowers the values of R_{on-s}, *SS*, and gate leakage current. Nevertheless, MIS-HEMT B exhibits a lower degradation rate in various device properties at high temperatures compared to MIS-HEMT A, indicating that ALD-Al_2O_3 passivation improves the thermal stability of device. The leading conduction mechanisms for the gate leakage current in our devices have been identified and can be ascribed to the combined effects of PF emission (Region I), TAT (Regions II and IV), and DAT (Region III).

See the supplementary material for details of XPS, temperature-dependent DC output/transfer characteristics, and gate leakage current and current collapse characteristics of *in-situ* SiN_x/AlN/GaN epilayer/MIS-HEMTs.

This research/project is supported by A*STAR under the RIE2025 Manufacturing, Trade, and Connectivity Programmatic Fund (Award M21K6b0134), and also, NRF and A*STAR under the RIE2025 White Space-MTC funding (Grant No. M23WSNG001).

AUTHOR DECLARATIONS

Conflict of Interest

The authors have no conflicts to disclose.

Author Contributions

Pradip Dalapati: Conceptualization (lead); Device fabrication (lead); Characterizations (lead); Data curation (lead); Investigation (lead); Methodology (lead); Validation (lead); Writing—original draft (lead); Writing—review and editing (lead). **Subramaniam Arulkumaran:** Data curation (supporting); Validation (equal); Writing – review & editing (supporting). **Hanlin Xie:** Characterizations (supporting); Data curation (supporting); Validation (equal); Writing—review and editing (supporting). **Geok Ing Ng:** Methodology (equal); Data curation (supporting); Funding acquisition (lead); Resources (lead); Supervision (lead); Project administration (lead); Validation (equal); Writing—review and editing (supporting); Coordinated the work and contributed to manuscript review.

DATA AVAILABILITY

The data that support the findings of this study are available from the corresponding author upon reasonable request.

REFERENCES

[1] Y. H. Chen, J. Encomendero, C. Savant, V. Protasenko, H. G. Xing, and D. Jena, Appl. Phys. Lett. **124**, 152111 (2024).
[2] G. Guodong, D. Shaobo, L. Yuanjie, H. Tingting, X. Peng, Y. Jiayun, and F. Zhihong, J. Semicond. **34**, 114004–114006 (2013).
[3] J. Yuan, G. J. Jing, J. C. Wang, L. Wang, R. H. Gao, Y. C. Zhang, Y. X. Yao, K. Wei, Y. K. Li, and X. J. Chen, J. Infrared Millim. Waves **43**, 200 (2024).
[4] P. Dalapati, H. Li, S. Arulkumaran, and G. I. Ng, Appl. Surf. Sci. **681**, 161532 (2025).
[5] A. Shanbhag, F. Grandpierron, K. Harrouche, and F. Medjdoub, Appl. Phys. Lett. **123**, 142102 (2023).
[6] L. Yang, W. Huang, D. Wang, B. Zhang, Y. Zhang, J. Zhang, T. Chen, W. Ge, S. Wu, B. Shen, and X. Wang, ACS Appl. Electron. Mater. **5**, 4786−4791 (2023).
[7] H. Xie, Z. Liu, W. Hu, Y. Gao, H. T. Tan, K. E. Lee, Y. X. Guo, J. Zhang, Y. Hao, and G. I. Ng, Appl. Phys. Express **15**, 016503 (2022).
[8] J. Ma, X. Lu, H. Jiang, C. Liu, and K. M. Lau, Appl. Phys. Express **7**, 091002 (2014).
[9] H. Jiang, C. Liu, Y. Chen, X. Lu, C. W. Tang, and K. M. Lau, IEEE Trans. Electron Devices **64**, 832–839 (2017).
[10] R. Natarajan, P. Murugapandiyan, S. Chinnaswamy, and N. Vigneshwari, Investigate AlN/GaN HEMT performance for future RF and high voltage switching applications, *2*024 International Conference on Advances in Modern Age Technologies for Health and Engineering Science

(AMATHE), India, pp. 1−6 (2024), https://doi.org/10.1109/AMATHE61652.2024.10582210.
[11] A. Bose, D. Biswas, S. Hishiki, S. Ouchi, K. Kitahara, K. Kawamura, and A. Wakejima, IEEE Access **9**, 57046−57053 (2021).
[12] P. Dalapati, S. Urata, and T. Egawa, Superlattice. Microst. **147**, 106709 (2020).
[13] H. Lee, H. Ryu, and W. Zhu, Appl. Phys. Lett. **122**, 112103 (2023).
[14] J. Zhu, Q. Zhu, L. Chen, B. Hou, L. Yang, X. Zhou, X. Ma, and Y. Hao, IEEE Trans. Electron Devices **64**, 840–847 (2017).
[15] N. Said, K. Harrouche, F. Medjdoub, N. Labat, J. G. Tartarin, and N. Malbert, Thermal and statistical analysis of various AlN/GaN HEMT geometries for millimeter Wave applications, 2023 IEEE International Reliability Physics Symposium (IRPS), pp. 1–5, (2023), https://doi.org/10.1109/IRPS48203.2023.10117807.
[16] J. S. Xue, J. C. Zhang, and Y. Hao, Appl. Phys. Lett. **107**, 043503 (2015).
[17] S. Liu, Y. Zhuang, H. Li, Q. Xie, Y. Wang, H. Xie, K. Ranjan, and G. I. Ng, Appl. Phys. Lett. **125**, 023504 (2024).
[18] P. Dalapati, S. Arulkumaran, D. Mani, H. Li, H. Xie, Y. Wang, and G. I. Ng, Mater. Sci. Eng. B **307**, 117503–117512 (2024).
[19] Z. Xu, J. Wang, Y. Cai, J. Liu, Z. Yang, X. Li, M. Wang, M. Yu, B. Xie, W. Wu, X. Ma, J. Zhang, and Y. Hao, IEEE Electron Device Lett. **35**, 33–35 (2014).
[20] Y. J. Lu, Z. H. Feng, Z. J. Lin, H. Y. Guo, G. D. Gu, J. Y. Yin, Y. G. Wang, P. Xu, X. B. Song, and S. J. Cai, Chin. Phys. **23**, 077105 (2014).
[21] A. J. Tzou, K. H. Chu, I. F. Lin, E. Østreng, Y. S. Fang, X. P. Wu, B. W. Wu, C. H. Shen, J. M. Shieh, W. K. Yeh, C. Y. Chang, and H. C. Kuo, Nanoscale Res. Lett. **12**, 315 (2017).
[22] X. Tan, Y. Lu, G. Gu, L. Wang, S. Dun, X. Song, H. Guo, J. Yin, S. Cai, and Z. Feng, J. Semicond. **36**, 074008 (2015).
[23] L. Deng, L. Zhou, H. Lu, L. Yang, Q. Yu, M. Zhang, M. Wu, B. Hou, X. Ma, and Y. Hao, Micromachines **14**, 2104 (2023).
[24] N. E. Grant, S. L. Pain, E. Khorani, R. Jefferies, A. Wratten, S. McNab, D. Walker, Y. Han, R. Beanland, R. S. Bonilla, and J. D. Murphy, Appl. Surf. Sci. **645**, 158786 (2024).
[25] X. Lu, K. Yu, H. Jiang, A. Zhang, and K. M. Lau, IEEE Trans. Electron Devices **64**, 824–831 (2017).
[26] J. Bernat, P. Javorka, A. Fox, M. Marso, H. Luth, and P. Kordos, Solid-State Electron **47**, 2097–2103 (2003).
[27] B. Luo, R. Mehandru, J. Kim, F. Ren, B. P. Gila, A. H. Onstine, C. R. Abernathy, S. J. Pearton, D. Gotthold, R. Birkhahn, B. Peres, R. C. Fitch, N. Moser, J. K. Gillespie, G. H. Jessen, T. J. Jenkins, M. J. Yannuzi, G. D. Via, and A. Crespo, Solid-State Electron **47**, 1781–1786 (2003).
[28] S. Arulkumaran, Z. H. Liu, G. I. Ng, W. C. Cheong, R. Zeng, J. Bu, H. Wang, K. Radhakrishnan, and C. L. Tan, Thin Solid Films **515**, 4517–4521 (2007).
[29] Y. Shi, W. Chen, R. Sun, C. Liu, Y. Xia, Y. Xin, X. Xu, F. Wang, X. Deng, T. Chen, and B. Zhang, IEEE Trans. Electron Devices **66**, 4164–4169 (2019).
[30] A. D. Koehler, N. Nepal, T. J. Anderson, M. J. Tadjer, K. D. Hobart, C. R. Eddy, and F. J. Kub, IEEE Electron Device Lett. **34**, 1115–1117 (2013).
[31] X. Ding, L. Song, G. Yu, Y. Cai, Y. Sun, B. Zhang, Z. Du, Z. Zeng, X. Zhang, and B. Zhang, Mater. Sci. Semicond. Process. **162**, 107502 (2023).
[32] Y. Xing, Z. Han, X. Huang, G. Yu, C. Yin, B. Guan, J. Han, B. Zhang, and Z. Zeng, Microelectron. Reliab. **151**, 115263 (2023).
[33] S. Arulkumaran, T. Egawa, H. Ishikawa, and T. Jimbo, Appl. Phys. Lett. **82**, 3110–3112 (2003).
[34] Y. Li, G. I. Ng, S. Arulkumaran, G. Ye, Z. H. Liu, K. Ranjan, and K. S. Ang, J. Appl. Phys. **121**, 044504 (2017).
[35] M. Kumar, V. Khandelwal, S. Yuvaraja, D. Chettri, H. Cao, G. Mainali, X. Tang, and X. Li, Jpn. J. Appl. Phys. **63**, 100905 (2024).
[36] S. Turuvekere, N. Karumuri, A. Azizur Rahman, A. Bhattacharya, A. DasGupta, and N. DasGupta, IEEE Trans. Electron Devices **60**, 3157–3165 (2013).
[37] G. Dutta, N. DasGupta, and A. DasGupta, IEEE Trans. Electron Devices **64**, 3609–3615 (2017).
[38] Z. H. Liu, G. I. Ng, S. Arulkumaran, Y. K. T. Maung, and H. Zhou, Appl. Phys. Lett. **98**, 163501 (2011).
[39] C. h. Chen R. Sadler, D. Wang, D. Hou, Y. Yang, W. Yau, S. Wang, M. Wu, T. Wu, R. Chen, and B. Ou, The interplay of thermal, time and Poole-Frenkel emission on the trap-based physical modeling of GaN HEMT drain characteristics, 2017 IEEE Compound Semiconductor Integrated Circuit Symposium (CSICS), USA, 2017, pp. 1–4, https://doi.org/10.1109/CSICS.2017.8240427.
[40] Z. Ouennoughi, C. Strenger, F. Bourouba, V. Haeublein, H. Ryssel, and L. Frey, Microelectron. Reliab. **53**, 1841–1847 (2013).
[41] X. Lu, J. Ma, H. Jiang, and K. M. Lau, Appl. Phys. Lett. **104**, 032903 (2014).
[42] S. Huang, Q. Jiang, S. Yang, C. Zhou, and K. J. Chen, IEEE Electron Device Lett. **33**, 516–518 (2012).